Monthly Notices
of the
ROYAL ASTRONOMICAL SOCIETY

MNRAS **434,** 2907–2921 (2013) doi:10.1093/mnras/stt1199
Advance Access publication 2013 August 14

EISCAT observations of meteors from the sporadic complex

Noah Brosch,[1]★ Ingemar Häggström[2] and Asta Pellinen-Wannberg[3]

[1]*The Wise Observatory and the Raymond and Beverly Sackler School of Physics and Astronomy, the Faculty of Exact Sciences, Tel Aviv University, Tel Aviv 69978, Israel*
[2]*EISCAT Scientific Association and Swedish Institute of Space Physics, Box 812, S-981 28 Kiruna, Sweden*
[3]*Umeå University and Swedish Institute of Space Physics, Box 812, S-981 28 Kiruna, Sweden*

Accepted 2013 June 27. Received 2013 June 27; in original form 2013 March 3

ABSTRACT

We report meteor observation with the European Incoherent Scatter Scientific Association (EISCAT) radars obtained during a continuous 24-h period in 2009 December. The period, just after the Geminid meteor shower, was selected to have no strong meteor shower activity to allow a comparison with our previous observations collected during the 2008 Geminid shower. During the 2009 run, we used the very high frequency (VHF) and ultrahigh frequency systems, but most of the results presented here were derived from the VHF data. We discuss the statistical properties of the radar echoes, their Doppler velocity and altitude distributions, their radar cross-section, etc. We concentrate, as in our previous paper, on the population of high-altitude echoes, which we clearly detect, and discuss these specifically. We recognize a few echoes with positive Doppler velocities as produced by meteoroids that presumably entered the atmosphere at ∼grazing incidence angles and were leaving it when detected by radar. We detect meteor echoes with essentially zero Doppler velocity, reported here for the first time, which we interpret as meteoroids moving almost perpendicular to the beam and producing specular reflections off the meteor trail. We discuss meteors detected with tristatic measurements for which we find bunching in azimuth and depression angle that depends on the time of the day. Finally, we report again of the lack of extreme velocity meteors, a fact that weakens significantly the claim of the existence and abundance of interstellar meteors.

Key words: techniques: radar astronomy – meteorites, meteors, meteoroids.

1 INTRODUCTION

The atmospheric entry of high-velocity meteoroids produces ionized plasma trails that reflect radio waves and typically last less than one second. Radio reflections from meteoric trails can appear as radar echoes at many wavelengths. They can, in principle, belong to two categories: 'head echoes' produced by reflection off the shock front immediately preceding the meteoroid and by the plasma created in the immediate vicinity of the meteoroid, and 'trail echoes' produced by the plasma left after the meteoroid passage. Meteor echoes can, in principle, be detected at high frequency, very high frequency (VHF) and ultrahigh frequency (UHF). The plasma generation is primarily attributed to the ablation of meteoroid material at altitudes below ∼130 km produced by heating from the shock front (e.g. Popova, Strelkov & Sidneva 2007) and by meteoroid sputtering at higher altitudes (Brosch et al. 2001, Schijvarg 2006). In both cases, the ionized material originates from the meteoroid as well as from the ambient atmosphere.

Traditionally, radar meteor observations are aimed at altitudes below 130 km within the typical 'meteor layer', but radar meteor campaigns at ∼1 GHz with a much wider range gate reported by Brosch et al. (2001) identified two populations of meteor radar echoes, one corresponding to the classical region of meteoroid ablation at 80 to 130 km and another at much higher altitudes, peaking at ∼250 km. Unfortunately, given the classified nature of the military phased-array high-power radar (PAR) systems used for these observations, only fragmentary results from these observations could be published. For this reason, we decided to probe the same high-altitude meteor population using unclassified high-power large-aperture radar (HPLAR) systems available to the scientific community. Most such installations do not have the advantage of PAR systems such as used for the observations reported by Brosch et al. (2001); those can scan quasi-instantaneously ∼ π steradians with their synthesized beams, but classical HPLARs are limited by the rather narrow single beam of a non-tracking dish antenna.

Meteors have been observed with the HPLAR at EISCAT for more than a decade (Pellinen-Wannberg & Wannberg 1994) where the difference between incoherent scatter echoes from the F region and meteors was pointed out. We reported previously on EISCAT HPLAR observations of meteors with the UHF and VHF radars,

★ E-mail: noah@wise.tau.ac.il

at frequencies 930 MHz and 224 MHz, respectively (Brosch et al. 2010). Briefly, the 2008 observations bracketed the peak activity of the Geminid meteor shower with the intention of exploring, in addition to the high-altitude meteor population, the influence of the Geminid shower on meteor rates. During that run, we detected 11 radar echoes above 150 km among more than 22 000 VHF echoes but, since the range gate for the 2008 observations was set at 50 to 250 km, we missed resolving the 250-km peak of the second high-altitude distribution that was measured in our previous observations. We also did not detect an enhancement of the echo rate near the peak of the shower, indicating that most echoes we detected belonged to the sporadic population.

The large sample of VHF meteors as well as the smaller UHF sample showed higher Doppler velocities in the morning hours than around local midnight. However, since the observations were performed on three different days on the nights of 2008 December 11–12, 12–13 and 13–14, with the radars operating from 23:00 local (22:00 UT) until 07:00 local (06:00 UT) the following morning, we could not address possible variations in meteor rates with time of the day outside the eight-hour observation window.

The observations proposed for 2009 aimed to go well past 250 km, to identify the second peak in the altitude distribution and to detect a clear decrease of echo numbers above 250 km. The proposed range gate allowed an overlap with the 2008 results and extended the explored altitudes. Since it is possible that high-altitude echoes are not produced by meteor showers but by sporadic meteors, we asked to schedule the proposed 2009 observations for an intershower period.

Preliminary results from our 2009 observing run were already described by Häggström et al. (2010) and the full results are presented here. This paper is structured as follows: we discuss the experimental setup in Section 2 and the data analysis in Section 3. The results are presented in a series of subsections in Section 4 and are discussed in Section 5. The last section summarizes the paper.

2 EXPERIMENT

The observations were conducted from 10:30 UT on 2009 December 17 to 11:00 UT the following day, covering 24.5 h with only a few short interruptions. The transmitting and receiving was done from the EISCAT Ramfjordmoen site near Tromsø, Norway, with both VHF and UHF antennas pointed to the zenith. The 3 dB (50 per cent) beam size of the VHF system is $1\overset{\circ}{.}5 \times 1\overset{\circ}{.}7$ corresponding to a sky area of $\sim$2.8 km^2 at an altitude of 100 km. The corresponding size for the UHF system has a diameter of $0\overset{\circ}{.}6$ corresponding to a sky area of $\sim$0.4 km^2 at an altitude of 100 km. Two additional UHF receiving stations, at Kiruna (Sweden) and Sodankylä (Finland), were used to provide tristatic UHF capability, as done for the 2008 run. The difference for 2009 was that the three-beam common volume was set at an altitude of 102 km above Tromsø.

The experimental setup used for the 2009 observations was almost identical to that used during the previous run, therefore many technical details will not be repeated here; the interested reader may check our first EISCAT paper (Brosch et al. 2010). The few differences are pointed out and discussed below.

In order to improve the detectability of high-altitude echoes, we used the MANDA-4 setup normally used for ionospheric observations. The MANDA 'meteor code' was modified by increasing the interpulse period so that meteor detection could be achieved up to altitudes of $\sim$300 km. This setup uses an interpulse time of 2.5 ms and a 64-bit alternating code where each bit is 4 μs long. The code cycles every 0.32 s; this implies that by decoding the echoes on a bit-by-bit basis, range aliasing appears only for targets more distant than 48000 km.

The echoes are sampled at 250 kHz for the VHF and 500 kHz for the UHF when using the binned analysis (see below), and the resultant spectra cover the frequency range $\pm 40\,\mathrm{km\,s^{-1}}$ for the UHF and $\pm 84\,\mathrm{km\,s^{-1}}$ for the VHF. For approaching meteors, the velocity range covered by the UHF system is thus 0–81 $\mathrm{km\,s^{-1}}$ due to frequency aliasing, and is 0–167 $\mathrm{km\,s^{-1}}$ for the VHF.

3 ANALYSIS

In the experiment, the radio waves are scattered by the electrons in the plasma. This is essentially what is done when probing the ionosphere by radar. During the observing run in 2009 December the geomagnetic conditions were quiet, thus a number of persistent layers could form. These, and the regular ionospheric activity, determine the background against which meteor echoes have to be detected. As it will be shown below, in a number of cases and at certain times during the run, the contribution from the persistent layers affected the detectability. Fig. 1 shows the behaviour of the ionosphere above Tromsø during the run as a grey-scale plot of electron density versus altitude and time, with darker shades representing higher electron densities (see grey-scale at the right of the figure). The dark areas between 200 and 300-km altitude extending over noon from the beginning of the observation to about 15 UT (16 LT), and in the morning from about 8 UT (9 LT) to the end of the run, represent the normal sun-lit day-time maximum ionization in the F region. After 19 UT there is some auroral precipitation reaching down to 110-km altitude resulting probably from diffuse aurora.

Fig. 1 also exhibits some interesting features in the E region. Note first the 'fluffy' lace present at 90 to 100 km from the beginning of the observation till about 18 UT, then from about 22 to 3 UT; these are low-altitude sporadic E layers. Also, some meteor head echoes are visible just as single dots or short vertical lines below 100-km altitude with the highest range resolution. A third slightly stronger sporadic E layer is induced by a tidal semidiurnal wave descending from the F region around midnight and is seen and enhanced from 4 to 6 UT at about 105-km altitude. This elevated background level caused a reduction in the event rates seen during this period, as will be explained below. Due to the lower height resolution the fine structure of this layer is hidden by the 4-km vertical resolution in the plot.

The analysis presented here was performed with two independent methods. The first one uses an EISCAT-standard common programme mode. The value of this method is that it can be used by anybody and the data can be freely downloaded and studied with existing analysis programs. Even long-term studies can be performed using old data as well as ongoing common program runs. This method was used also for the 2008 observations described in Brosch et al. (2010) and is called here 'binned analysis'. The analysis uses data integrated over 1.6 s intervals; this is the duration of each EISCAT data dump. A careful frequency analysis detects the meteor echoes. The method is fast and accurate, and yields total reflected power, Doppler velocity, Doppler width and height of the echo. Sometimes there might be more than one meteor event in a data dump; while this pile-up caused the loss of some meteor events in the analysis of the 2008 run, this problem was fixed for the 2009 run.

The second method used is, so far, a research group method and is not generally available. It is included here only as a test and is used to select promising echoes for further investigation. The method is called here 'raw data analysis' (RDA), and uses a different receiver

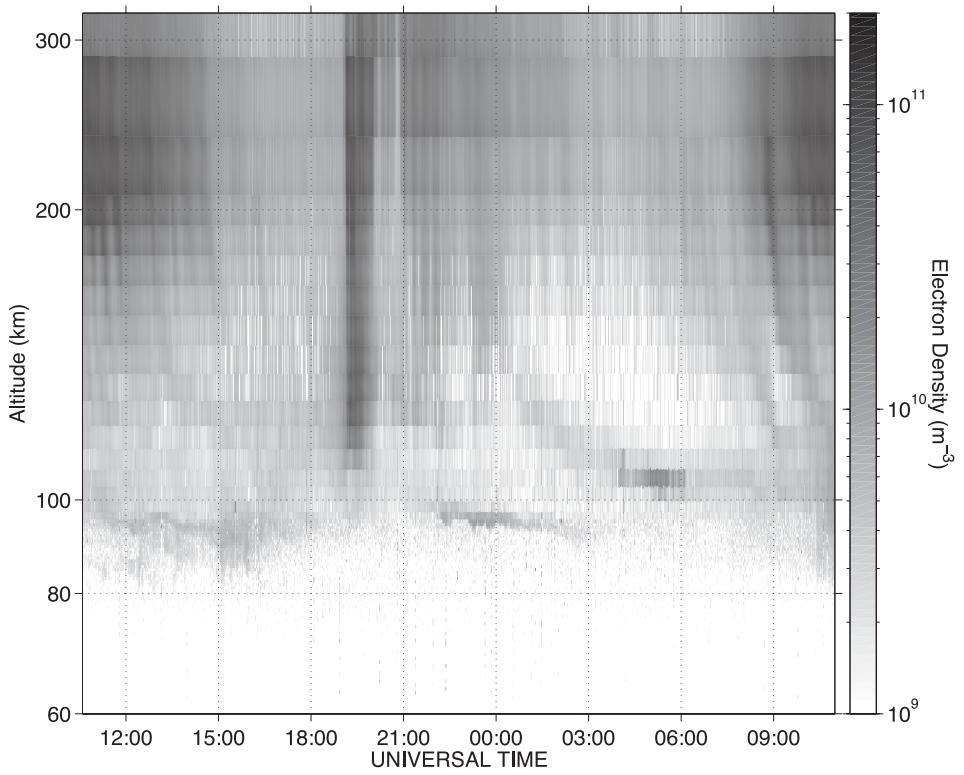

Figure 1. Time description of the electron density versus altitude at zenith over Tromsø, for the duration of the EISCAT VHF run described here. The electron density is coded with the grey-scale at right and runs from 10^9 to 2×10^{11} m^{-3}. Note that the vertical scale is logarithmic.

chain in which the raw incoming radar samples are recorded at a higher data rate than used for the binned analysis. The VHF echoes are sampled at 1 MHz and the VHF ones at 2 MHz using a Universal Software Radio Peripheral device. Continuous-time raw voltage samples were stored on a hard drive for offline processing – this data stream also included samples of the radar transmission envelope, which allowed us to correct for any amplitude and phase drift caused by the radar's high-power amplifier. This results in unaliased Doppler velocity estimates of $\pm 335\,\mathrm{km\,s^{-1}}$ (VHF) and $\pm 161\,\mathrm{km\,s^{-1}}$ (UHF).

The recorded samples are analysed offline one by one; this requires significantly more computer power but yields additional information such as the duration of each echo. It also allows the detection of meteor echoes at zero Doppler velocity and yields about twice as many detections as the first method. The target detection algorithm was implemented using the NVidia GTX295 graphical accelerator card, which allowed near real-time analysis speeds for the full-bandwidth raw voltage data.

The RDA method is based on the maximum likelihood estimation of three moving point-target parameters: range, velocity and radar cross-section (RCS). This involves the coherent integration of single radar pulses using a filter bank that is matched to the time-of-flight delayed radar transmission envelope and Doppler shift. The method was described by Markkanen, Lehtinen & Landgraf (2005) in the context of measurements of space debris. For meteors, the method is nearly identical to that for space debris, except that the accelerations and velocities involved are much larger and more variable. For this reason, only short coherent integration times, restricted to one transmission pulse, can be used in the detection stage.

Most recent meteor papers based on EISCAT data have however been based on another research group method. The radar code and its implementation was described in Wannberg et al. (2008). This method became possible after rebuilding the signal processing systems of the EISCAT mainland facilities and the first runs were performed during the vernal equinox 2002. In this method, raw data was used to reach very high simultaneous time (milliseconds) and spatial resolution and the velocities can be estimated both from the Doppler shift as well as from time of flight. A unique fragmentation event and orbital distribution of meteoroids in the Solar system were described in Kero et al. (2008). A recent review of the method was given by Pellinen-Wannberg (2011).

Real meteor echoes are picked from the data by selecting echoes with signal power above a certain threshold. We also require that there would be several echoes close in time, with similar range and Doppler characteristics. The individual detection are then combined into a meteor trajectory, for which a second-order polynomial function $R(t) = r_0 + v(t - t_0) + \frac{1}{2}a(t - t_0)^2$ is fitted, which allows us to obtain an estimate of the first three Taylor series coefficients of the target's radial trajectory. In order to obtain a more accurate acceleration estimate, we also fit the time-varying Doppler shift to the polynomial $\dot{R}(t) = v + a(t - t_0)$. To derive most of the results reported below we selected the output of this binned data analysis method.

4 RESULTS

At this point we discuss first the issue of sidelobes of the EISCAT VHF radar, since in certain conditions this could negatively have an impact on the detection of high-altitude echoes and was one of the objections raised in our previous paper.

In dealing with the positive Doppler velocity echoes, and particularly with the high-altitude ones, one should always consider the possibility of instrumental effects such as radar sidelobe effects. The antenna pattern of the EISCAT VHF system was studied by

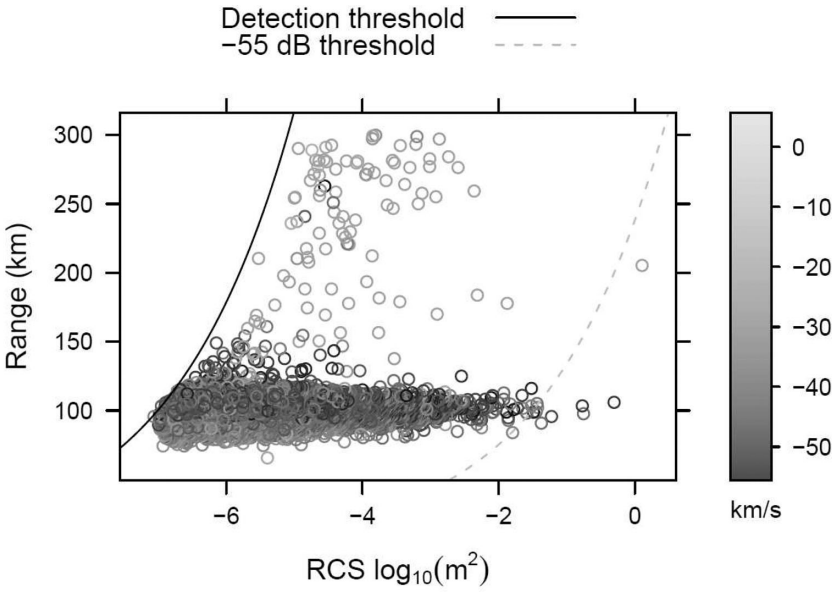

Figure 2. Echo range versus RCS. The solid line is the detection limit for objects at the zenith while the dashed line is for a −55 dB detection limit. The dots are various VHF detections from the run described here, coded for echo Doppler velocity in km s^{-1} with the grey-scale at right.

Kildal (1984). Kildal showed the beam pattern in the ∼east–west (E-W) and ∼north–south (N-S) directions from theoretical calculations combined with drift-scan measurements of Cas A. His plots, in particular those shown in his fig. 11, go out to ±45° in the N-S direction and ±30° in the E-W direction. These directions are explained in his fig. 4 and at the end of his section II.

'A beam pattern as a function of φ (azimuth angle) when α ('broadside angle') is constant is called a transverse beam pattern. This is the beam pattern of a cone with semi-cone angle $\theta = \pi/2 - \alpha$ about the z-axis (line feed axis). A longitudinal beam pattern is a beam pattern as a function of α for φ constant.'

The transverse direction lies therefore within a plane along the long axis of the trough antenna and approximately corresponds to the E-W direction; the longitudinal direction is ∼N-S. We write 'approximately' (∼) since Kildal's plots and coordinate system are tied to the VHF antenna, and the antenna is offset by 1° north towards west.

Kildal's (1984) plots show that, while the ∼N-S beam pattern has no significant sidelobes at large angles away from the beam centre at least within the range plotted in the paper, there are some worrisome sidelobes in the ∼E-W direction that originate from antenna structures. These sidelobes appear to be periodic, are ∼20 dB below the main beam, and do not decrease significantly with distance from the centre out to ±30° from the beam centre. The peaks, as read from Kildal's plots, are at about 11°.5, 13°, 15°.5, 18°.5, 21°, 26°.5 and 29° off the beam axis.

If this sidelobe pattern continues unchanged beyond a 30° off-axis direction, such sidelobes might introduce false echoes. However, the sidelobes appear only in the ∼E-W direction; the method of determining their nature lies in a comparison, for the same echo, of the data received through the N-S dipoles with that in the E-W dipoles. Since the Tromsø radar does not record separately the two polarizations, we cannot perform this comparison with the data we now have. With the setup used for the observations reported here the two polarizations are averaged, thus the Kildal (1984) sidelobes become ∼17 dB below the main lobe of the antenna.

An echo assumed to originate from meteor plasma at the zenith of Tromsø and detected at a range of ∼300 km may, in fact, result from the detection of a meteoroid at 100 km viewed in an antenna sidelobe at 70° zenith distance (20° elevation). To rule out such a possibility, we present in Fig. 2 the RCS versus range for all our detections, and on it we plot detection limits for the EISCAT VHF radar.

Fig. 2 shows two detection limits: one for objects at the zenith seen with the main beam, and another for a detection limit of −55 dB. This value was selected as a safe margin, by assuming that a sidelobe more distant than 30° off-beam would be ∼25 dB below the main lobe, which implies a returned signal through the same sidelobe to be ∼60 dB fainter than one transmitted and received through the main beam. The plot shows very few echoes to the right of the dotted line (with higher RCS, i.e. stronger); to be seen in a −55 dB sidelobe they would have to be very strong, thus very rare indeed. We conclude, therefore, that it is unlikely to have most of the apparent high-altitude echoes produced by transmitting through a distant sidelobe, reflecting off a ∼100-km meteor and receiving through the same distant sidelobe.

Summaries of the results for the VHF system used in this experiment are given in Figs 3–6. Fig. 3 shows in its top panel the number of echoes detected in each 30 min interval as a function of time during the experiment. The bottom panel of this figure shows the echo number density per km of altitude as a function of the altitude. Fig. 4 presents two histograms of echoes: the top panel plots the velocity distribution and the bottom panel gives the distribution of the signal-to-noise ratio (S/N) values of the echoes. Fig. 5 shows in the top panel the distribution of the range versus time. Since with the antenna pointing to the zenith range equals altitude, and after ruling out the sidelobe influence as explained above, this plot demonstrates directly the existence of high-altitude echoes. The bottom panel of this figure shows the distribution of velocities against time. Fig. 6 presents the distribution of ranges (altitudes) against the echo Doppler velocity in the top panel and, in the bottom panel, the distribution of the echo altitudes against acceleration.

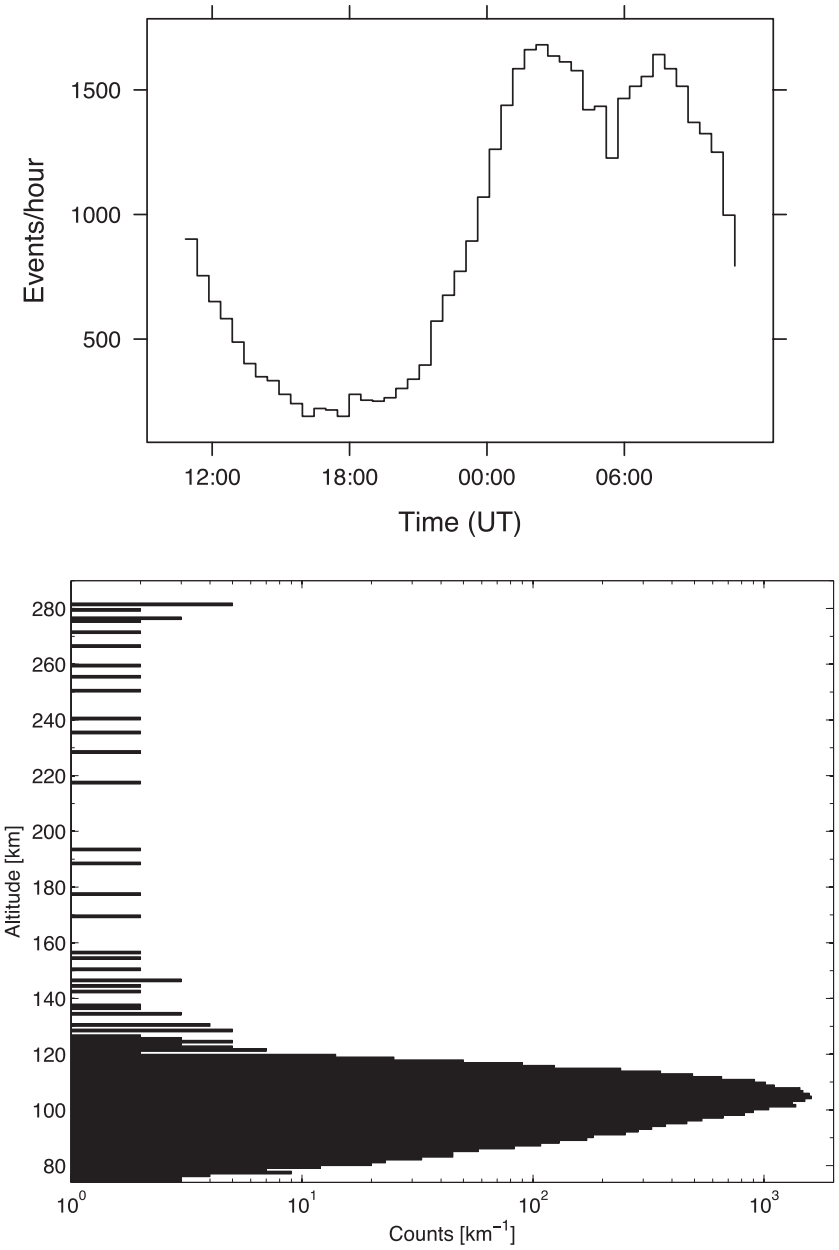

Figure 3. Summary of results for the VHF system. Top panel: detected echoes in a time histogram binned in 30 min intervals. Bottom panel: range histogram. Note that this plot is semilogarithmic; in order to emphasize the high-altitude echoes we plot the counts per altitude bin, on the horizontal scale, logarithmically.

4.1 Rates

The RDA yielded the highest meteor event rates with 23806 VHF echoes and 1565 UHF echoes. This is very similar to the total number of echoes reported during the 24 h non-consecutive observation in 2008 (Brosch et al. 2010). The binned method yielded only 12 522 VHF and 772 UHF echoes, probably because it rejected as invalid faint and short echoes, and was adversely affected by ionospheric features. This is almost the same UHF/VHF ratio, indicating no band-specific detection preference. The ∼16 times higher raw VHF rate, in comparison to the significantly lower UHF detection rate, is partly compensated by the different volumes sampled by the two beams. As shown in Brosch et al. (2010), the wider VHF beam has a seven times larger cross-sectional area than the UHF one. The difference of a factor of ∼2 between the beam-size-adjusted VHF and UHF rates indicates that there is only a weak wavelength dependency of the detection.

We did not find significant differences between meteor echoes detected by both methods in their significant parameters: a systematic velocity difference of ∼0.1 km s^{-1} and of 0.7 km in altitude, the latter attributed to the difference in the length of cabling between the feed and the different receivers.

Note the dip near 05:00 UT in the event rate versus time histogram evident in the top panel of Fig. 3. We estimate that it was caused by the increase in background noise caused by the persistent layer described above, which formed around that time and exhibited enhanced electron densities (see also Fig. 1); this reduced the S/N and 'drowned' some weak echoes. Below we describe briefly a few characteristic findings from the meteor echo analysis.

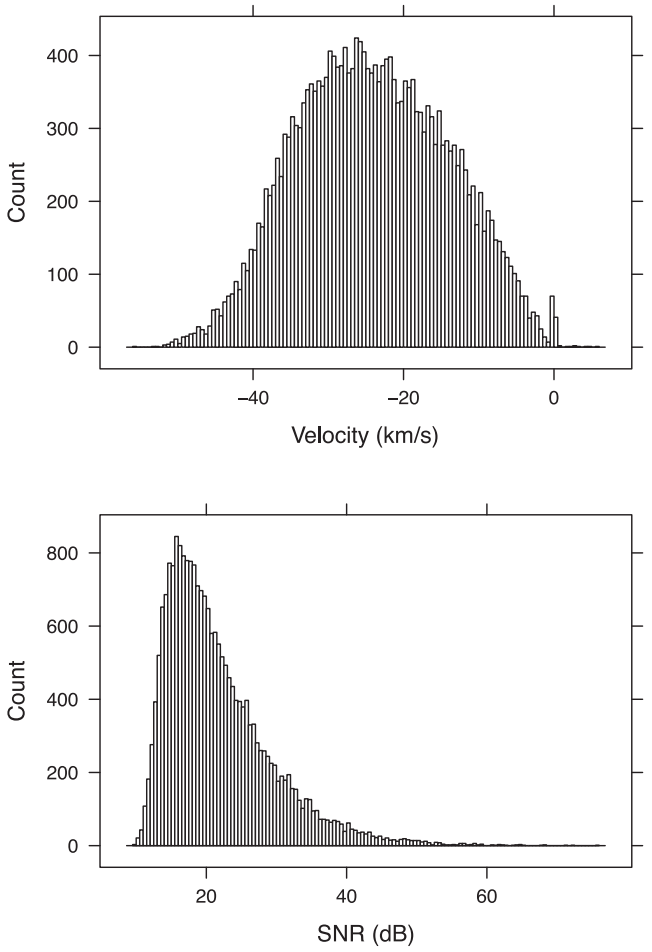

Figure 4. Summary results for the VHF system. Top panel: histogram of detected Doppler velocities. Bottom panel: S/N of the detections.

4.2 Altitude

Having shown that it is rather unlikely to have false detections of high-altitude meteors through very distant sidelobes, we now use 'altitude' for 'range' in the rest of the paper. The behaviour of various parameters such as those plotted in the bottom panel of Fig. 3 and top panel of Fig. 5, show some interesting findings. A number of high-altitude echoes, above 150 km, and an increase in the number of echoes above 200 km, are visible. Most high-altitude echoes show low to moderate incoming velocities (sometimes with positive Doppler), and only one echo shows both a high altitude (∼260 km) and a high incoming velocity (∼52 km s^{-1}).

The low-altitude echoes below ∼100 km show generally moderate to high deceleration (range rate) values, whereas the high-altitude echoes show exclusively rather low deceleration values ($\leq$25 km s^{-2}; bottom panel of Fig. 6), as could be expected given the much lower atmospheric density. The fastest meteor echoes are seen near the peak of the height distribution. The high-altitude VHF echoes, those above 130 km, are not visible in the UHF.

4.3 Distribution of echoes with time and echo duration

The almost continuous 24-h coverage, with no significant changes in the radar parameters, shows that more meteor echoes are detected in second half of the night with a strong minimum (for the VHF) between 15:00 and 20:00 local time (Fig. 3 top panel). This night peak is also visible in the UHF distribution but, due to the low statistics, the minimum is less well defined there than for the VHF echoes.

The two peaks shown in the plot of the meteor duration versus time (Fig. 7) are due to a combination of effects: longer duration echoes produced by higher incoming velocity in the morning, when the meteoroids tend to enter the atmosphere at high incidence angles (Apex source), and a longer dwell time of meteoroids in the beam with their velocity vector nearly aligned with the beam. In addition, evening meteoroids overtaking the Earth from behind have a lower velocity and thus also dwell longer in the beam. Moreover, the additional ionization during daytime (see Fig. 1) enhances the background against which the meteor echoes are detected. This reduces the detectability of faint echoes reducing the overall rate of radar meteor detection. This effect was already reported by Oppenheim et al. (2008), albeit for 50 MHz using the Jicamarca radar.

4.4 Velocity

The methods used here detect the velocity component along the beam using the Doppler shift of the transmitted frequency. Fig. 4 (top panel) indicates that no incoming velocities larger than about 60 km s^{-1} were measured. This was also the situation with the observations from 2008. We observed a number of instances of meteor echoes with positive Doppler velocities. These meteors were apparently moving away from the Earth, and were mostly at high altitudes. Examples are visible in the two summary plots in Fig. 5 (bottom panel) and Fig. 6 (top plot).

The Doppler velocity histogram in the top panel of Fig. 4 shows a clear but modest peak of echoes near zero Doppler; we discuss these events below. The bottom panel of this figure shows that most detected echoes have a reasonable S/N of ∼17, with no echo with S/N $\leq$ 10. Fig. 6 shows a significant number of echoes with ∼zero Doppler velocity in the top plot; these were distributed quite uniformly throughout the measurement range from ∼80 to ∼300 km. It is possible that these are meteors passing perpendicular to the beam and fulfilling the Bragg condition in order to become detectable.

4.5 Meteors and space debris

Another possible objection to the claim of the existence of high-altitude meteor echoes is that such echoes are caused by space debris from defunct satellites and rockets re-entering the atmosphere. There are two a priori arguments against this possibility: these cannot have Doppler velocities as high as the echoes detected here since orbital debris would move at typical orbital velocities or, at most, at free-fall velocities and such echoes would exhibit a much longer duration. The latter argument is because the typical time required to cross the beam for an object at 300 km, with a velocity similar to that of an orbiting object, is of the order of seconds whereas the detections presented here are one to two orders of magnitude shorter in time (see Fig. 7).

Moreover, we detected by chance the signature of a genuine orbital debris at ∼140 km adjacent in time to that of a 'real' high-altitude meteor echo at ∼295 km. These are presented in Fig. 8 where the difference between the two is clearly demonstrated. The orbital debris echo is visible from time 0 to 2.5 s whereas the meteor echo begins at the 3 s time mark and lasts for about 0.03 s. The first echo is prolonged and the signal strength oscillates; the range rate (velocity along the beam) is zero and does not change, showing that, for the time it was in the beam, the object producing the echo remained at ∼140 km. The meteor, on the other hand, shows a

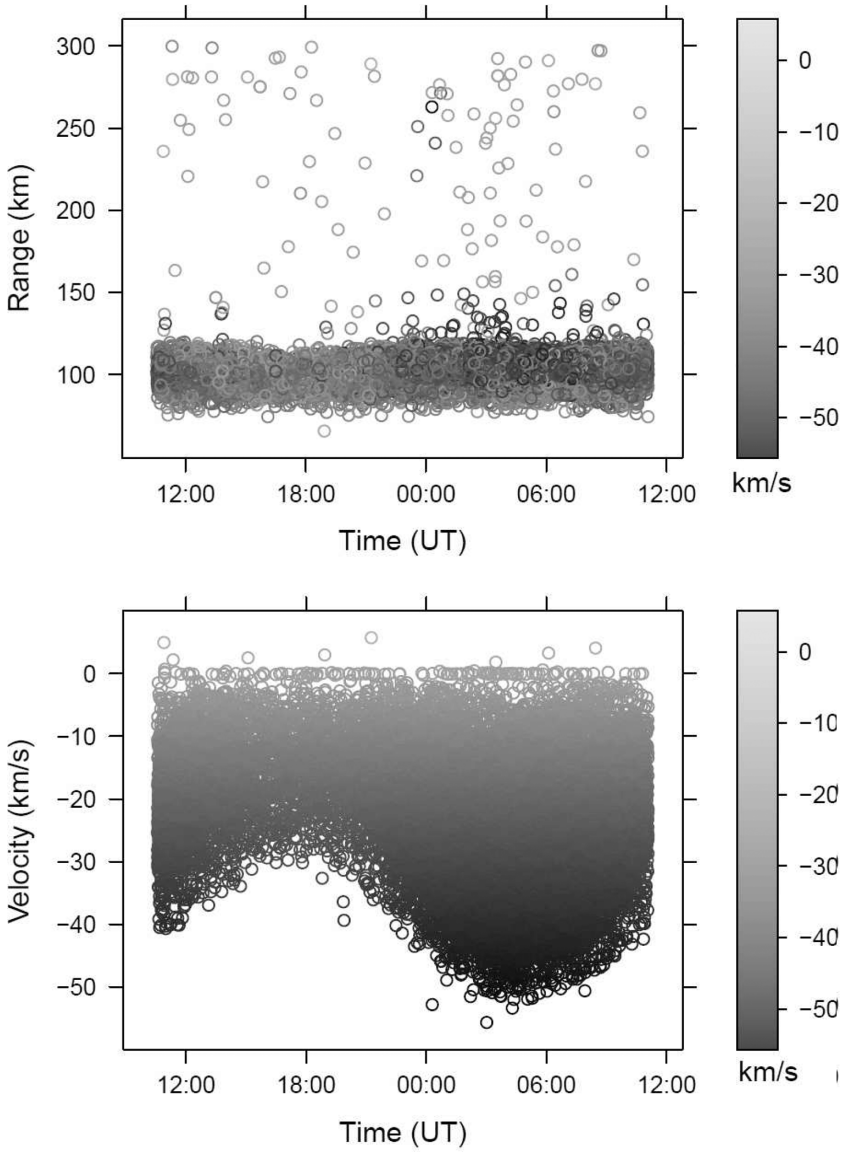

Figure 5. Summary of results for the VHF system. Top panel: detected echoes in range versus time. Bottom panel: Doppler velocity versus time. Note the coding of the echo Doppler velocities in km s^{-1}, given in the grey-scale on the right-hand side of each plot.

very short duration and a rapidly changing range. Since the debris signal was registered at ∼140-km altitude and lasted for at least 4 s, much longer than the beam transit time at that altitude for an object moving with orbital velocity, we suspect that it is really much more distant and has been range aliased.

The five panels of the figure plot every echo in the given time interval, produced using the RDA method described above, and show an expanded view of the changing range (altitude) against time plotted near the altitude of the meteor echo in the top-left panel. The entire range versus time is shown in the upper-right panel, the altitude-filtered range rate against time in the middle-left panel and the entire range rate against time in the middle-right panel again plotting every echo, and the power against time in the lower-left panel.

We show in Figs 9–12 examples of high-altitude echoes with relatively high velocity, and of low velocity meteors, one at a high altitude and the other at a lower altitude. The description of the different panels in these figures is like that given above for Fig. 8.

4.6 Tristatic detections

As already mentioned, the 2009 run was designed with the option of detecting the space motion of meteors passing at about 102-km altitude through the common volume sampled by the Tromsø UHF antenna located at 69°.59N, 19°.23E and the receiving stations in Kiruna, Sweden (67°.86N, 20°.44E) and Sodankylä, Finland (67°.36N, 26°.63E). The horizontal distances between these sites are 199 km for the Tromsø–Kiruna line and 391 km for the Tromsø–Sodankylä line. The receiving stations are 32-m diameter fully steerable dishes similar to the Tromsø UHF system and provide tristatic UHF capability over a rather limited atmospheric volume. Since their half-power (−3 dB) beams are ∼0°.7, they define the volume sampled by the three beams (∼6 km^3 for the Tromsø–Sodankylä volume at −3 dB).

Note that with tristatic observations, one considers first bistatic detections from two of the stations, then joint tristatic detections. After careful inspection of the echoes received in the satellite

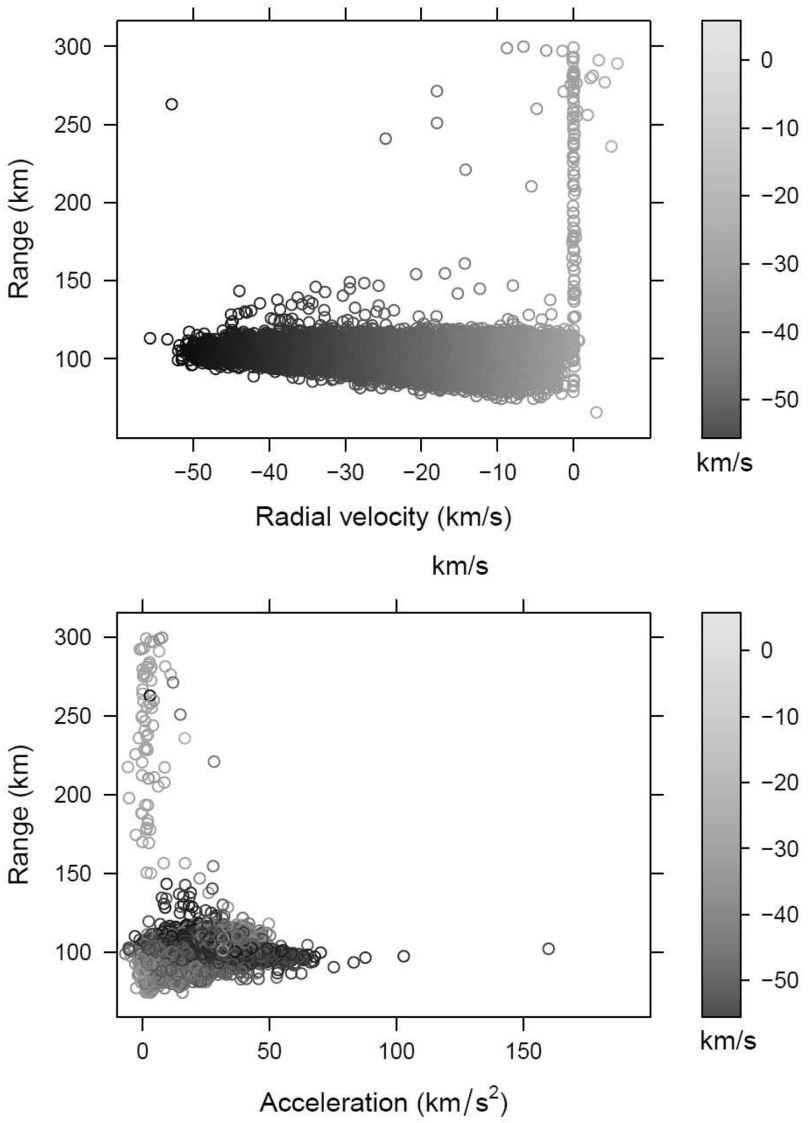

Figure 6. Summary results for the VHF system. Top panel: range versus Doppler velocity. Bottom panel: acceleration. The echo Doppler velocities are coded with the grey-scale in km s^{-1} at the right-hand side of each plot.

stations, 98 echoes that appeared on all three receiving stations were identified. This is in contrast with no tristatic echoes detected in 2008, when the common volume was set at 170 km above Tromsø, but keeping in mind that no UHF echoes were detected at high altitudes.

Tristatic EISCAT observations of meteors have been reported by e.g. Szasz et al. (2008b) and Kero et al. (2008). The review by Kero et al. mentions the detection of 410 tristatic events in four 24-h runs with the tristatic volume set at 96-km altitude, thus a rate of slightly more than four events per hour. We detect 98 events in 24.5 h at a slightly higher tristatic volume, implying a somewhat lower but comparable rate to the Kero et al. average. The experiments reported by Kero et al. used a different observation geometry, with the tristatic point set about half-way between the transmitter and the Sodankylä receiver to optimize the amount of tristatic events.

Note that Kero et al. (2008) actually detected only 65 meteors during their 24-h run near the winter solstice and this is what we should compare our measurements to, since radar meteor rates vary significantly with the season especially in the high polar latitudes. Our significantly higher rate of detections, when our 'aiming volume' was at a higher altitude than that of Kero et al., might indicate that the additional meteors we detected were at altitudes higher than 96 km and were missed by Kero et al.

Fig. 13 presents the derived measurable quantities for all 98 tristatic meteors in vectorial form (absolute value of the velocity and two angles: azimuth and elevation of the vector). It shows that there are not many tristatic meteors before midnight, and that those between midnight and close to dawn have a widely distributed azimuthal distribution while those in the morning are almost exclusively coming from the east. The reduction in the tristatic meteor rate during daytime is also probably related to the daytime ionization enhancement that enhances the background and hinders the detection of faint meteor echoes.

The figure shows that most tristatic echoes have been detected in the second half of the period after the local midnight. While the echoes before dawn exhibit a large azimuth (θ) and depression angle

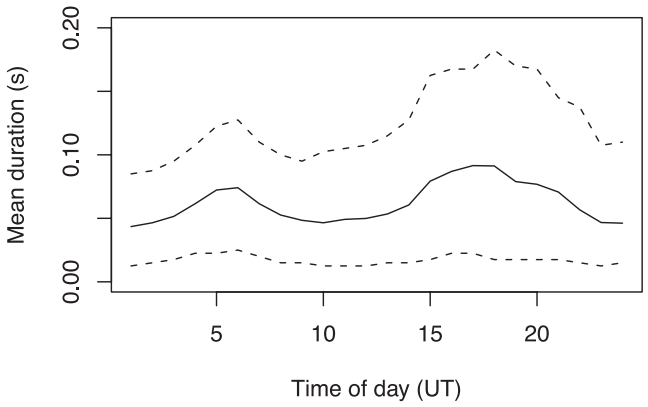

Figure 7. Mean duration of a meteor echo as a function of time of day (for convenience, the end of the run was plotted at the start of the plot to yield a continuous 24-h plot). The solid line is the mean and the two dashed lines mark the outermost ±10 per cent deviations from the mean (90 per cent of the echoes being within the two dashed lines). This corresponds to a bit less than a 2σ limit for a normal distribution. The morning peak is due to a higher relative velocity with respect to the Earth, while the afternoon peak is due to echoes being longer as the meteoroids overtake the Earth. The meteor rates are binned into 1-h bins.

(ϕ), those after 06:00 UT have a generally easterly azimuth and their depression angle ϕ decreases steadily from dawn at about -60° to approximately -20° close to noon. As far as we are aware, this has not been reported previously. The typical velocity increases with time from ∼18:00 UT to the end of the observations. This is the result of observing the faster morning side Apex population of mostly retrograde meteoroids, as observed also by Szasz et al (2008b). The depression angle ϕ decreases with time from about midnight UT to the end of the observations, when meteors are only $\sim 30^\circ$ below horizontal. The azimuthal angle θ increases steadily from a southerly direction near 19:00 UT to ∼east by 10:00 UT.

5 DISCUSSION

Our observations took place near the 2009 winter solstice. The zenith-pointing beams of the Tromsø systems point towards high ecliptic latitudes near midnight, but towards morning, as the Earth spins eastward by almost 120°, the vertical beams approach the ram direction of the orbital motion and the ecliptic latitude becomes lower. The Northern Toroidal source of sporadic meteors probably

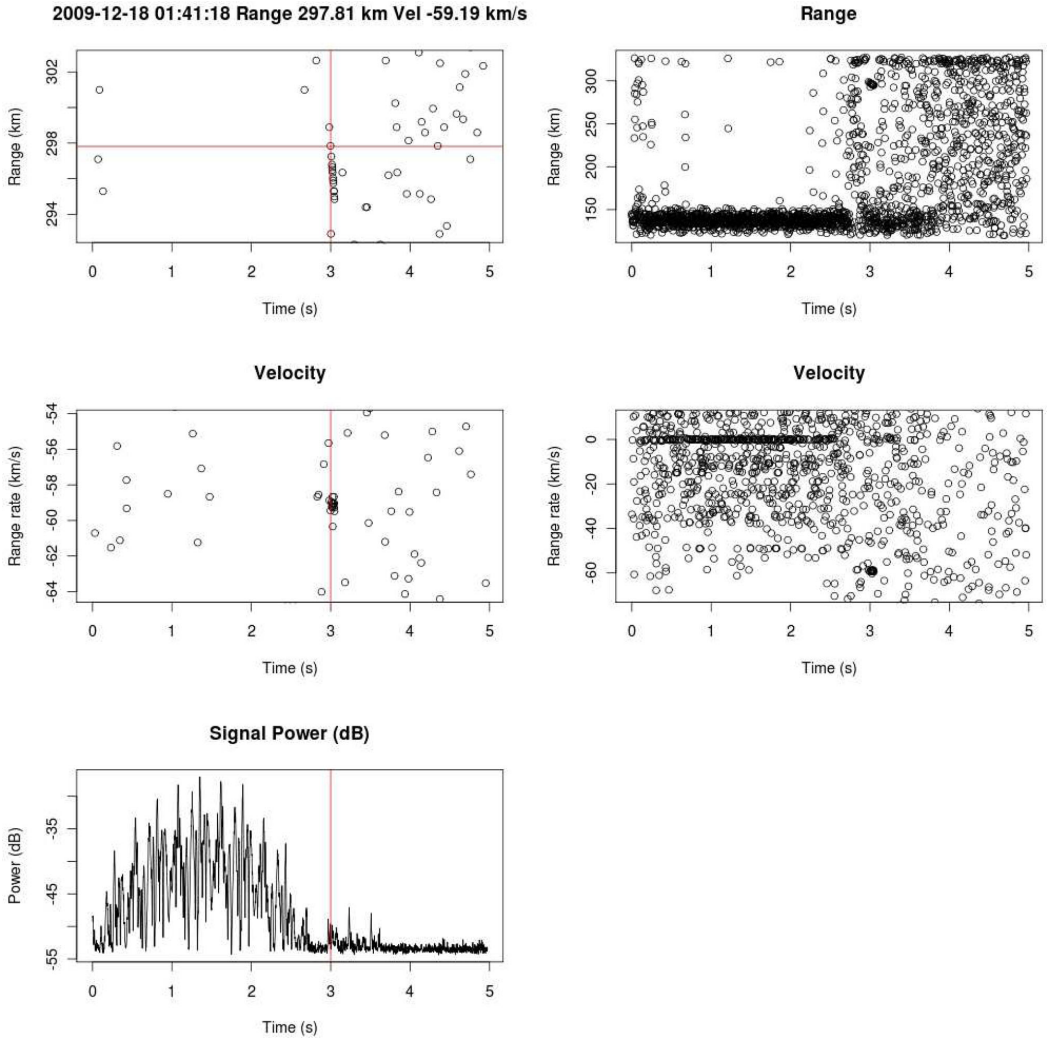

Figure 8. Signature of an orbital debris object at ∼140 km, adjacent to that of a ∼298-km meteor echo. While the track of the meteor, extracted with the RDA method, is short and has a Doppler velocity of –59 km s^{-1}, the signature of the space debris shows a Doppler velocity ∼0 km s^{-1} and a long and oscillating power output.

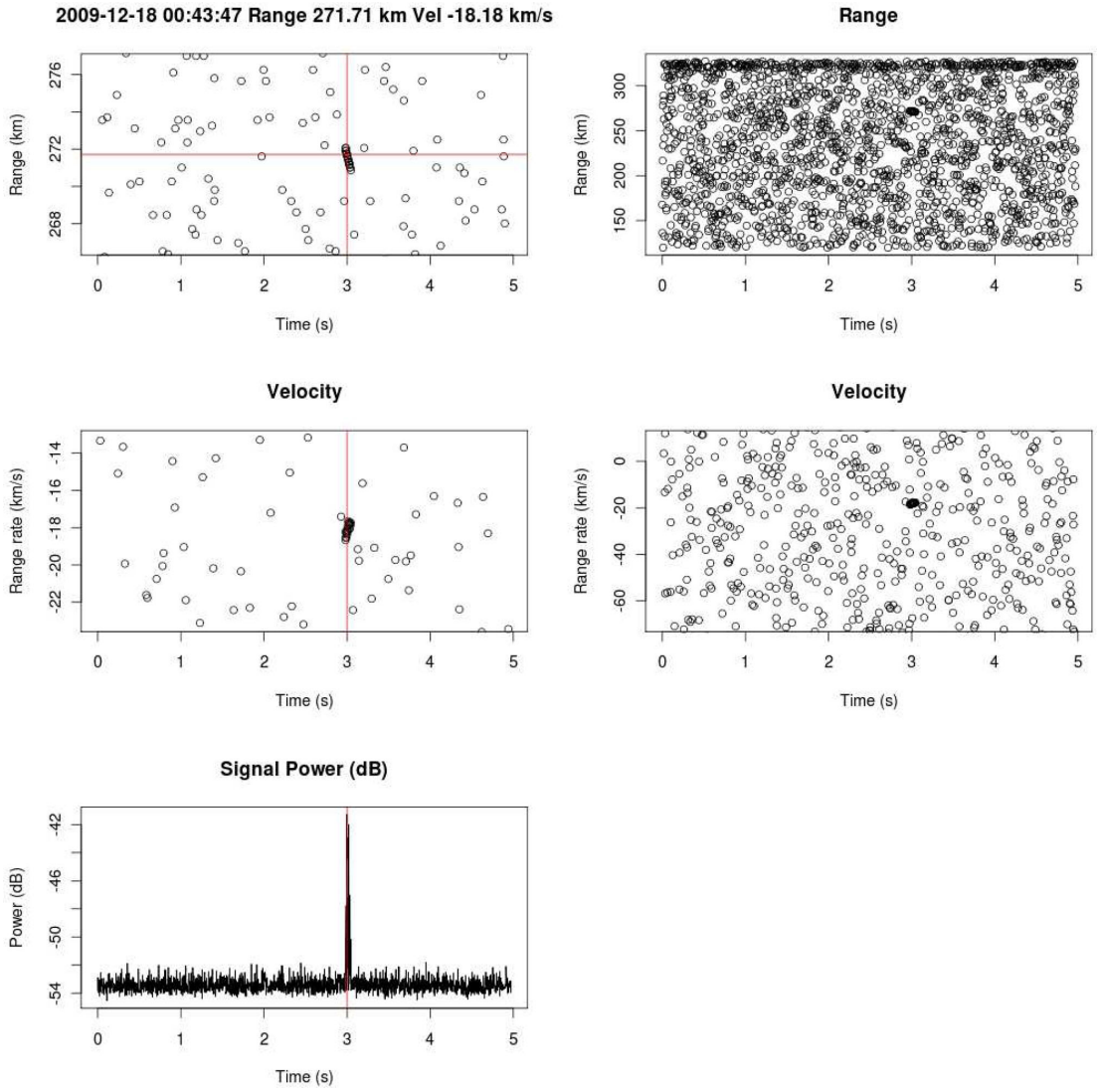

Figure 9. Example of a meteor echo at about 274 km and a velocity of $\sim$18 km s^{-1}.

becomes important at this time and the Earth's orbital motion adds to the vector of the meteoroid velocity.

The rate of radar meteors from a relatively high-latitude site (Juliusruh in northern Germany: 54°.63N, 13°.40E; radar operating at 32.55MHz and with a range gate 78–120 km) was studied by Szasz et al. (2004). They found that, for five days around the winter solstice, the echo rates peaked near 04:00 local time and reached a (single) minimum near local noon. A similar result, with a lower amplitude, was obtained for the ESRANGE radar operating near Kiruna (67°.88N, 21°.12E).

More meteor echoes were detected in second half of the night with a strong minimum (for the VHF) between 15:00 and 20:00 local time (Fig. 3 top panel). The rate enhancement is the result of the orientation of the radar beam, always pointed to the local zenith, which comes close to the velocity vector of the Earth's orbital motion (Apex) at this time, and is also observed for visual and TV-detected meteors. This result is essentially identical to that of Szasz et al. (2004) and has already been discussed by Szasz et al. (2008b).

The two peaks in the echo duration versus time of day plot, shown in Fig. 7, are due to longer echoes produced by the higher incoming velocity in the morning, when meteoroids tend to hit the atmosphere at high incidence angles, and to evening meteoroids overtaking the Earth from behind.

5.1 High-altitude echoes

Fig. 3 bottom panel and Fig. 5 top panel demonstrate the existence of significant numbers of high-altitude echoes, higher than 150 km and appearing as high as 300 km; they also show an enhancement in echo numbers with altitude above 200 km. Although some might consider it suspicious that many of the high-altitude echoes have near-zero Doppler velocities, we explained above that these might have trajectories $\sim$perpendicular to the beam while fulfilling the Bragg condition. We also gave a few detailed examples of high altitude but low-Doppler echoes to demonstrate their reality. This hints at the presence of a second peak in the meteor altitude distribution that was identified in Brosch et al. (2001). Specifically, the bottom panel of Fig. 3 shows that most echoes do belong to the 'classical' meteor layer, at $\sim$70 to 130-km altitude, with a decreasing tail to about 160 km. Above this altitude and up to the limit of the distribution sampled here there are scattered echoes at various altitudes

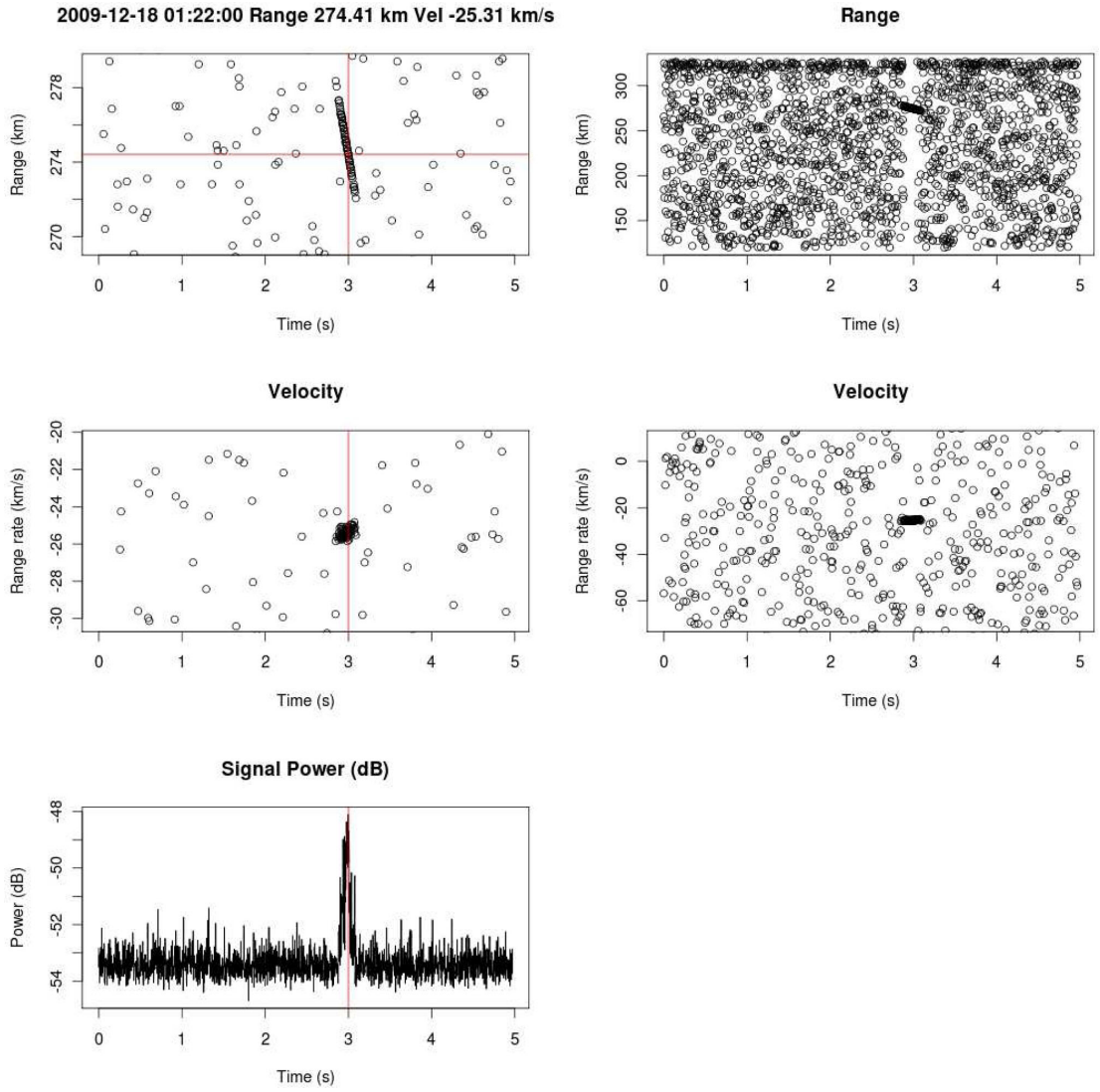

Figure 10. Another example of a high-altitude meteor echo, at approximately the same altitude as the meteor in Fig. 9, with a velocity of $\sim$25 km s^{-1}.

with an enhancement near the top of our altitude range; the confirmation of this finding would require further observations that reach to even higher altitudes.

Fig. 6 (top plot) shows also a significant number of echoes at altitudes above 130 km; these are the high-altitude ones to which the experiment was tuned and which were mentioned previously. By roughly binning the echoes higher than 150 km into two bins, we can firmly establish the existence of the second peak in the altitude distribution of meteor echoes. The bin from 150 to 225 km has only 35 echoes, while that from 225 to 300 km has 58.

The existence of meteor plasma at high altitudes was traditionally dismissed, because the tenuous atmosphere there could not have supported the traditional meteor ablation mechanism, assumed to be the only one producing meteor plasma. We find it interesting that the idea of plasma production by meteoroid sputtering at high altitudes became accepted by the community following our 2001 paper. As Mendis & Maravilla (2009) have shown, electrons can be produced by sputtering at altitudes above 140 km, reaching as high as 280 km (see their fig. 1a).

5.2 Decelerating meteors

The bottom panel of Fig. 6 shows the run of the acceleration (actually deceleration) with altitude. For most meteor echoes at altitudes up to $\sim$130 km the acceleration can have any value from negative (boosting out) to decelerating at up to 100 km s^{-2} = 10^4 g! The high-altitude echoes, however, show exclusively low to moderate accelerations, up to $\sim$25 km s^{-2} and most decelerating at $a \leq 10$ km s^{-2}. This is expected for the high-altitude population, given the low atmospheric density that results in low drag.

The echo showing the strongest acceleration is a 'meteor layer' object at $\sim$100 km decelerating with 170 km s^{-2}. Note also that the deceleration values discussed here, with the exception of the tristatic meteors, relate to only one component of the deceleration vector; the one along the beam. This is, therefore, a lower limit to the deceleration.

We interpret echoes with positive velocities as produced by meteoroids on grazing-incidence trajectories that do not penetrate sufficiently deep into the atmosphere to be slowed down significantly, and 'bounce back' into deep space. Such events are known

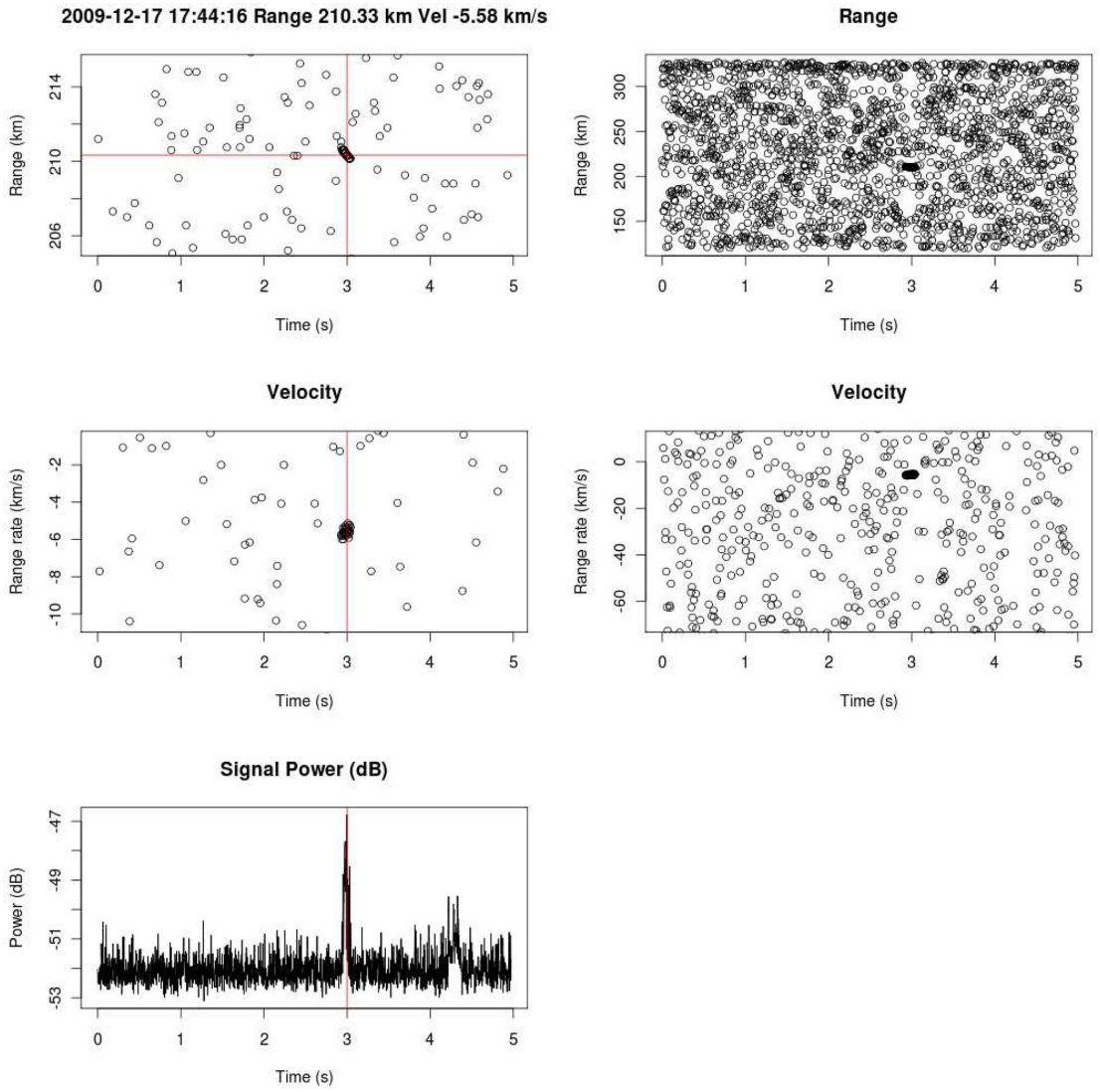

Figure 11. Example a meteor echo at a high altitude (∼210 km) but with a low velocity of ∼5.6 km s^{-1}.

from optical observations; e.g. the Great Daylight 1972 Fireball (or US19720810), a large meteoroid that passed within 57 km of the surface of the Earth on 1972 August 10 and returned to space.

Moreover, we report for the first time on the detection of meteor echoes with ∼zero Doppler velocity. These stand out in the top panel of Fig. 6, and their range values show that they can be detected at all altitudes, up to 300 km. We propose that those are cases in which we detect specular reflection off meteor trails (or elongated head echoes) that pass overhead of Tromsø perpendicular to the beam.

5.3 Shower versus non-shower meteor activity

Meteor showers are not expected to greatly influence radar meteor counts. Szasz et al. (2008a) found that most radar meteors with reliable orbits from tristatic UHF observations did not originate from extrasolar locations or had asteroidal origins; short-period comets could be the dominant source for these meteoroids. About 40 per cent of the radiants could be associated with the North Apex sporadic meteor source and 58 per cent of the orbits were retrograde. We, therefore, expected that many of the meteors we would detect would also belong to the sporadic population. Chau & Woodman (2003) did not detect Leonid shower meteors with the Jicamarca HPLAR and concluded that these were a negligible addition to the echoes they detected.

Chau & Galindo (2008) detected meteor echoes from the η Aquarid and from the Perseid showers with a HPLAR (Jicamarca, at 50 MHz). They mentioned that, lacking interferometric capabilities for the HPLAR, it would be difficult to identify echoes as belonging to showers and not to the sporadic population based only on their velocity distributions. Shower meteors were apparently recognized also in data taken with the MU radar, another HPLAR with interferometric capabilities (Kero et al. 2010) and are clearly visible in fig. 2 of Kero et al. (2011).

5.4 Interstellar meteors?

The question of the existence and detectability of 'interstellar' (IS) meteors has long been discussed in the astronomical literature (e.g. Opik 1950). In most cases, IS meteors are recognized by their velocity. The detected meteor velocity is a combination of the orbital motion of the meteor and that of the Earth. The

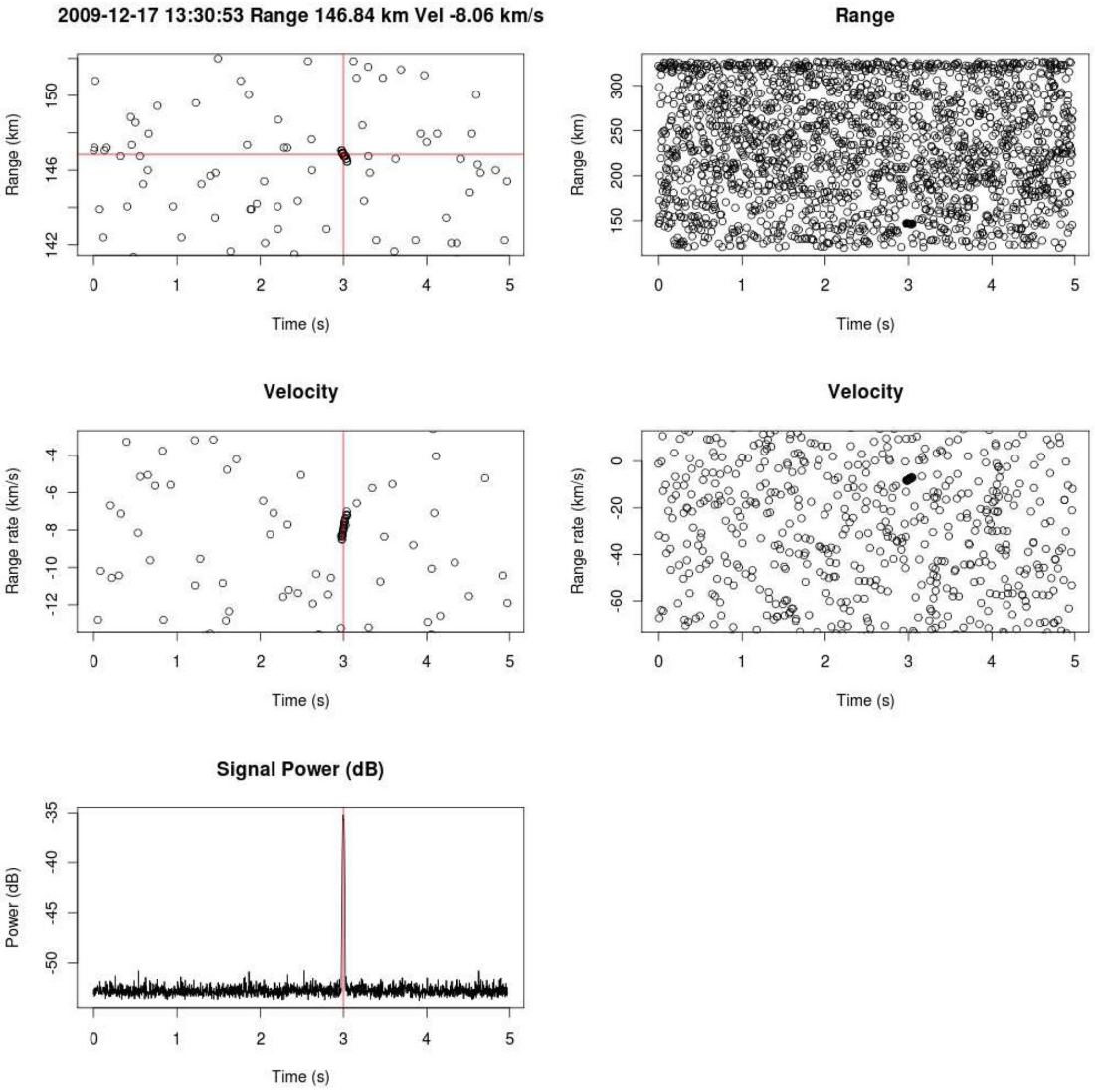

Figure 12. Another example of a meteor echo with a low velocity of $\sim$8 km s^{-1} at a lower altitude than the meteor of Fig. 11.

Earth orbits the Sun at $v_{\oplus} \sim 29.7\,\mathrm{km\,s^{-1}}$, and the highest velocity a body in the Earth neighbourhood can have and still be orbiting the Sun is $v_{\mathrm{parabolic}} \sim 42.1\,\mathrm{km\,s^{-1}}$. Therefore, the fastest Solar system meteor, which encounters the Earth 'head-on', can move with $v_{\oplus} + v_{\mathrm{parabolic}} = 71.8\,\mathrm{km\,s^{-1}}$. Objects with significantly higher velocities are candidates for IS meteors.

Hawkes & Woodworth (1997a) discussed the question of optical IS meteors and even claimed the detection of two such meteors (Hawkes & Woodworth 1997b). Grün & Landgraf (2000) studied the influence of collisions on the size distribution of IS grains. They concluded that large grains can exist for a long time, and can travel considerable distances ($\sim$1 kpc) within the Milky Way disc before they are destroyed.

Baggaley et al. (2005) argued that meteoroids larger than about 1 μm (4×10^{-12} g) can enter the inner Solar system and, upon encountering the Earth, produce meteors. Krüger et al. (2007) reviewed the question of IS dust in the Solar system based on data from the dust impact detectors operating on-board interplanetary probes (e.g. Ulysses). They found that IS grains with masses up to 10^{-13} kg penetrate deep into the system and that their flow direction is close to the mean apex of the Sun"s motion.

Meisel, Janches & Mathews (2002) identified slightly more than 100 echoes ($\sim$3 per cent) received in 1997–1998 by the Arecibo radar as having an IS origin. The authors suggested that the Geminga supernova could be the likely source or transport agent. Later, Meisel et al. (2004) justified the lack of additional detections of IS meteors with Arecibo as the influence of Jupiter moving into the IS dust stream.

The collection of four IS dust particle candidates by the Stardust Aerogel Interstellar Dust Collector was recently claimed by Westphal et al. (2011, 2012). The claim is based on the trajectories being approximately consistent with an origin in the IS dust stream with its radiant at galactic longitude $\sim$270°, similar to previous derivations from Ulysses and Galileo impact measurements.

As already stated here, as well as in our previous paper, no incoming velocities above 72 km s^{-1} (here not even above $\sim$60 km s^{-1}) were measured implying the extreme rareness of IS meteors. This lack of IS meteors is strengthened when the present result is combined with results from our previous run. Specifically, with more than 4×10^4 meteor echoes detected, there was not even one with $v > 72\,\mathrm{km\,s^{-1}}$. In fact, the highest Doppler incoming velocities were 54 km s^{-1} in 2008 and 56 km s^{-1} in 2009. This dearth of high

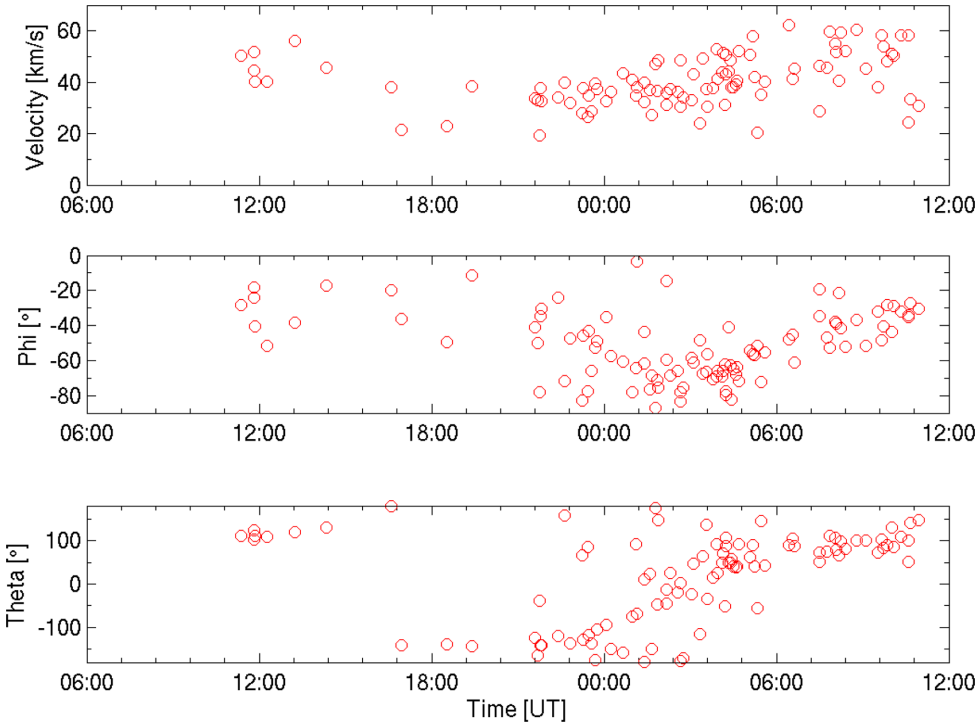

Figure 13. Tristatic meteors; parameters versus time. The absolute value of the velocity is in the top panel. The elevation (actually the depression) angle ϕ is in the middle panel and is always negative since these are descending meteors, and the azimuthal angle θ is in the bottom panel with zero at north and positive to the east.

incoming velocity echoes from objects that could be IS meteors is in contrast with previous claims by e.g. Baggaley (2004), Close (2004), Baggaley et al. (2005) about detecting meteor echoes with hyperbolic velocities. Our finding may serve to put the matter of hyperbolic IS meteors at rest.

6 SUMMARY

(i) We reported observations with EISCAT performed in 2009 December to monitor radar meteor activity over a 24-h period.

(ii) We detected more than 22 000 VHF echoes and about a tenth that much in UHF.

(iii) The high statistics show a clear tendency for increased meteor rates in the morning hours, with Doppler velocities higher than at other times of the day.

(iv) We showed that a small number of meteor echoes are due to incoming meteoroids at grazing incidence, detected when leaving the atmosphere.

(v) The tristatic UHF observations detected 98 echoes appearing in all three receiving stations: Tromsø, Kiruna and Sodankylä, similar to what was already detected at EISCAT by Szasz et al. (2008b).

(vi) We detected and reconfirmed the existence of a population of high-altitude radar meteors first identified by Brosch et al. (2001), above 130 km, with echoes reaching as high as ∼300 km.

(vii) We failed to detect echoes with Doppler velocities in excess of ∼60 km s^{-1} at any time during the 24-h observation. This, combined with a similar negative result from our 2008 observations, puts a serious question mark on the existence of radar meteors that originate from IS space and are detected at hyperbolic velocities.

ACKNOWLEDGEMENTS

NB is grateful to the EISCAT management and to its Trans-National Access programme (TNA) for support towards the 2009 observing run. We gratefully acknowledge the EISCAT staff for their assistance during the observation campaigns. EISCAT is an international association supported by research organizations from China (CRIPR), Finland (SA), Germany (DFG), Japan (NIPR and STEL), Norway (NFR), Sweden (VR) and the United Kingdom (STFC). We acknowledge the outstanding contribution to this paper by Juha Vierinen.

REFERENCES

Baggaley W. J., 2004, Earth Moon Planets, 95, 197
Baggaley W. J., 2005, LPI Contribution. No. 1280, Lunar and Planetary Institute, Houston, Texas, p. 23
Brosch N., Schijvarg L. S., Podolak M., Rosenkrantz M. R., 2001, ESA SP-495: Meteor Observations from Israel. ESA, Noordwijk, p. 165
Brosch N., Häggström I., Pellinen-Wannberg A., Westman A., 2010, MNRAS, 401, 1069
Chau J. L., Galindo F., 2008, Icarus, 194, 23
Chau J. L., Woodman R. F., 2003, Atmos. Chem. Phys. Discuss., 3, 6063
Close S., 2004, PhD thesis, Boston University
Grün E., Landgraf M., 2000, J. Geophys. Res., 105, 10291
Häggström I., Pellinen-Wannberg A., Westman A., Vierinen J., Brosch N., 2010, Eur. Geosci. Union Gen. Assem., 12, 9601
Hawkes R. L., Woodworth S. C., 1997a, J. R. Astron. Soc. Can., 91, 68
Hawkes R. L., Woodworth S. C., 1997b, J. R. Astro. Soc. Can., 91, 218
Kero J., Szasz C., Wannberg G., Pellinen-Wannberg A., Westman A., 2008, Geophys. Res. Lett., 35, 7101
Kero J. et al., 2010, COSPAR Sci. Assem., 38, 1223
Kero J. et al., 2011, MNRAS, 416, 2550
Kildal P.-S., 1984, IEEE Trans. Antennas Propag., 32, 541

Krüger H., Landgraf M., Altobelli N., Grün E., 2007, Space Sci. Rev., 130, 401
Markkanen J., Lehtinen M., Landgraf M., 2005, Adv. Space Res., 35, 1197
Meisel D. D., Janches D., Mathews J. D., 2002, ApJ, 567, 323
Meisel D. D., Bartlett B. D., Mathews J. D., Janches D., Briczinski S., 2004, BAAS, 36, 779
Mendis D. A., Maravilla D., 2009, Geophys. Res. Lett., 36, L22804
Opik E. J., 1950, Ir. Astron. J., 1, 80
Oppenheim M. M., Sugar G., Bass E., Dimant Y. S., Chao J., 2008, Geophys. Res. Lett., 35, L03102
Pellinen-Wannberg A., 2011, Radio Sci. Bull., 339, 32
Pellinen-Wannberg A., Wannberg G., 1994, J. Geophys. Res., 99, 11379
Popova O. P., Strelkov A. S., Sidneva S. N., 2007, Adv. Space Res., 39, 567
Schijvarg S., 2006, PhD thesis, Tel Aviv University
Szasz C., Kero J., Pellinen-Wannberg A., Mathews J. D., Mitchell N. J., Singer W., 2004, Earth Moon Planets, 95, 101
Szasz C., Kero J., Pellinen-Wannberg A., Meisel D. D., Wannberg G., Westman A., 2008a, Earth Moon Planets, 102, 373
Szasz C., Kero J., Meisel D. D., Pellinen-Wannberg A., Wannberg G., Westman A., 2008b, MNRAS, 388, 15
Wannberg G., Westman A., Kero J., Szasz C., Pellinen-Wannberg A., 2008, Ann. Geophys., 26, 2303
Westphal A. J. et al., 2011, LPI Contribution No. 1608, 42nd Lunar and Planetary Science Conference. Lunar and Planetary Institute, Houston, Texas, p. 2083
Westphal A. J. et al., 2012, LPI Contribution No. 1659, 43rd Lunar and Planetary Science Conference. Lunar and Planetary Institute, Houston, Texas

This paper has been typeset from a TEX/LATEX file prepared by the author.